

Contents

Legend	3
1 The Algorithm	7
1.1 Step So0: Prepare Data	7
1.2 Step So1b: Find Mean Rossby Radii and Phase Speeds	8
1.3 Step So2: Calculate Geostrophic Parameters	8
1.4 Step So3: Find Contours	9
1.5 Step So4: Filter Eddies	9
1.6 Step So5: Track Eddies	18
1.7 Step So6: Cross Reference Old to New Indices	20
2 Results	23
2.1 MI - 7 day time-step - AVISO	25
2.2 MII - 7 day time-step - AVISO	30
2.3 MII - 7 day time-step - POP	32
2.4 MII - 7 day time-step - POP remapped to AVISO geometry	33
2.5 MII - 1 day time-step - POP	35
3 Discussion	37
3.1 Lengths of Tracks	37
3.2 Scales	38
3.3 Drift Speeds	40
4 Bibliography	47

Legend

Definition 1: Reynolds Number Re

Compares advection of momentum to frictional acceleration.

$$Re = \frac{UL}{\nu}$$

Definition 8: Buoyancy Vector $\mathbf{B} 1/\text{s}^2$

$$\mathbf{B} = -\frac{\nabla \rho \times \nabla p}{\rho^2}$$

Definition 2: Rossby Number Ro

Compares advection of momentum to Coriolis acceleration.

$$Ro = \frac{U}{fL}$$

Definition 9: Kinetic Energy per mass $E_k \text{m}^2/\text{s}^2$ **Definition 3: Rhines Number R_{fi}**

Ratio of Rhines scale to horizontal scale.

$$R_{fi} = \frac{U}{\beta L^2} = \frac{a}{L} Ro$$

Definition 10: Mechanical Energy per mass $E_k \text{m}^2/\text{s}^2$

Sum of kinetic and potential Energy.

Definition 11: Rossby Radius $L_R \text{m}$

The *geostrophic wavelength*. $L_R = c/f$

Definition 4: Burger Number Bu

Ratio of relative vorticity to *stretching* vorticity.

$$\sqrt{Bu} = \frac{NH}{fL} = \frac{L_R}{L}$$

Definition 12: Steering Level z_S

The critical depth where the real part of the Doppler shifted phase speed $c_S(z_S) = c(z) - u(z) = 0$ vanishes. I.e. the depth where the Doppler shift creates a standing wave, causing the disturbances to grow in place instead of spreading in space, analogous to a *supersonic bang*.

Definition 6: gravitational acceleration $g \text{ m/s}^2$

Value of surface normal component of all body forces.

Definition 7: vorticity $\omega \text{1/s}$

Definition 13: Rhines Scale L_{fi} [m]

Scale at which earth's sphericity becomes important.

$$L_{fi}^2 = \frac{U}{\beta} \quad (1)$$

Assuming Gaussian shape:

$$h = Ae^{-(x/\sigma)^2/2}$$

with $A = a' + a = Ae^{-1/2} + a$

$$\begin{aligned} \frac{\partial h(\sigma)}{\partial x} &= -\frac{A}{\sigma} e^{-1/2} \\ &= -\frac{a'}{\sigma} \end{aligned}$$

hence

$$\begin{aligned} L_{fi} &= \sqrt{\frac{g}{f} \frac{\partial h}{\partial x} \frac{1}{\beta}} \\ L_{fi} &= \sqrt{\frac{ga'}{f\sigma\beta}} \end{aligned} \quad (2)$$

TODO:en detail:

$$\begin{aligned} \frac{\partial h(\sigma)}{\partial x} &= -\frac{A}{\sigma} e^{-1/2} \\ &= -\frac{a}{\sigma} \frac{e^{-1/2}}{(1 - e^{-1/2})} \\ &= \frac{a}{\sigma(e^{1/2} - 1)} \end{aligned}$$

hence

$$\begin{aligned} L_{fi} &= \sqrt{\frac{g}{f} \frac{\partial h}{\partial x} \frac{1}{\beta}} \\ L_{fi} &= \sqrt{\frac{g}{e^{1/2} - 1} \frac{a}{f\sigma\beta}} \end{aligned} \quad (3)$$

Definition 14: Gravity Wave Phase Speed cm/s

$$c = \sqrt{g'H}$$

Definition 15: Reduced Gravity $g'(x,y,z)m/s^2$

$$\text{In the layered model } g' = g \frac{\delta\rho}{\rho_0} = N^2 h$$

Definition 16: Surface/interface Displacement $\eta(x,y)m$ **Definition 17: Brunt Väisälä frequency $N1/s$**

$$N^2 = g / \rho_0 \frac{\partial \rho}{\partial z}$$

Definition 18: Mean Layer thickness Hm **Definition 19: Layer Thickness/physical height of an isopycnal surface $h(x,y,t)m/h(x,y,\rho,t)m$**

$$h = H + \eta \text{ (in the layered model)}$$

Definition 20: Planetary Vorticity $\Omega1/s$

$$\Omega = 4\pi/\text{day}_{fix*}$$

Definition 21: Latitude ϕ rad

Definition 22: Earth's Radius a m**Definition 23: Surface-Normal Planetary Vorticity Component $f_{1/s}$**

$$f = \cancel{f} z = \Omega \sin \phi z$$

Definition 24: Change of Planetary Vorticity with Latitude β 1/ms

$$\beta = \frac{\partial f}{\partial y} = \Omega/a \cos \phi$$

Definition 25: Okubo-Weiss Parameter O_w 1/s²

$$O_w = \text{divergence}^2 + \text{stretching}^2 + \text{shear}^2 - \text{vorticity}^2.$$

A negative value indicates vorticity dominated motion, whereas a positive value indicates deformation.

Definition 26: Sea Surface Height SSH m**Definition 27: Isoperimetric Quotient IQ**

$$IQ = A/A_c = \frac{A}{\pi r_c^2} = \frac{4\pi A}{U^2} \leq 1.$$

The ratio of a ring's area to the area of a circle with equal circumference.

Definition 28: Gaussian radius r m

$$(H - a) = H \exp \left(-\frac{A}{2\pi r^2} \right).$$

Twice the Gaussian standard-deviation.

a : amplitude

H : Gaussian amplitude

A : determined area

Definition 29: dynamic eddy scale σ m

Distance from eddy's center to the line of maximum orbital speed *i.e.* the zero-vorticity contour.

Definition 30: Run **aviso-MI**

7-day time-step aviso with method **MI**.

Definition 31: Run **aviso-MII**

7-day time-step aviso with method **MII**.

Definition 32: Run **pop2avi-MII**

7-day time-step POP remapped to aviso-geometry with method **MII**.

Definition 33: Run **POP-7day-MII**

7-day time-step POP with method **MII**.

Definition 34: Run **POP-1day-MII-Southern-Ocean**

1-day time-step aviso with method **MII**.

Southern Ocean Only.

Minimum Age: 30 [d]

Contour step raised to 2 [cm]

1

The Algorithm

This section walks through the algorithm step by step, so as to explain which methods are used and how they are implemented. The idea is that the code from step `S00..on` can only accept one well defined structure of data. In earlier versions the approach was to write code that would adapt to different types of data automatically. All of this extra adaptivity turned out to visually and structurally clog the code more than it did offer much of a benefit. The concept was therefore reversed. `S00_prep_data` can be altered to produce required output. Yet, there should be no need to adapt any of the later steps in any way. All input parameters are to be set in `INPUT.m` and `INPUTXXX.m`.

1.1 Step S00: Prepare Data

```
function S00_prep_data
```

Before the actual eddy detection and tracking is performed, SSH-, latitude- and longitude-data is extracted from the given data at desired geo-coordinate bounds and saved as structures in the form needed by the next step (S01). This step also builds the file `window.mat` via `GetWindow3` which saves geometric information about the input and output data as well as a cross-referencing index-matrix which is used to reshape all *cuts* to the user defined geo-coordinate-geometry. The code can handle geo-coordinate input that crosses the longitudinal seam of the input data. E.g. say the input data comes in matrices that start and end on some (not necessarily strictly meridional) line straight across the Pacific and it is the Pacific only that is to be analyzed for eddies, the output maps are stitched accordingly. In the zonally continuous case *i.e.* the full-longitude case,

an *overlap* in x-direction across the *seam*-meridian of the chosen map is included so that contours across the seam can be detected and tracked across it. One effect is that eddies in proximity to the seam can get detected twice at both zonal ends of the maps. The redundant *ghost*-eddies get filtered out in `S05_track_eddies`.

1.2 Step S01b: Find Mean Rossby Radii and Phase Speeds

```
function S01b_BruntVaisRossby
```

This function...

- – ...calculates the pressure $P(z, \phi)$ in order to...
 - ...calculate the Brunt-Väisälä-Frequency according to $N^2(S, T, P, \phi) = -\frac{g(\phi)}{P} \frac{\partial \rho(S, T, P)}{\partial z}$ in order to...
- – ...integrate the Rossby-Radius $L_R = \frac{1}{\pi f} \int_H N dz$ and ...
 - apply the long-Rossby-Wave dispersion relation to found L_R to estimate Rossby-Wave phase-speeds $c = -\frac{\beta}{k^2 + (1/L_r)^2} \approx -\beta L_R^2$

The 3-dimensional matrices (S and T) are cut zonally into slices which then get distributed to the threads. This allows for matrix operations for all calculations which would otherwise cause memory problems due to the immense sizes of the 3d-data ¹.

¹ E.g. the pop data has dimensions $42 \times 3600 \times 1800$.

1.3 Step S02: Calculate Geostrophic Parameters

```
function S02_infer_fields
```

This step reads the cut SSH data from `S00_prep_data` to perform 2 steps:

1. Calculate a mean over time of $SSH(y, x)$.
2. • use one of the files' geo-information to determine f , f_i , g and the ratio g/f .
 - calculate geostrophic fields from SSH gradients.
 - calculate deformation fields (vorticity, divergence, stretch and shear) via the fields supplied by the last step.
 - calculate O_w .
 - Subtract the mean from step 1 from each $SSH(t)$ to filter out persistent SSH-gradients e.g. across the Gulf-Stream.

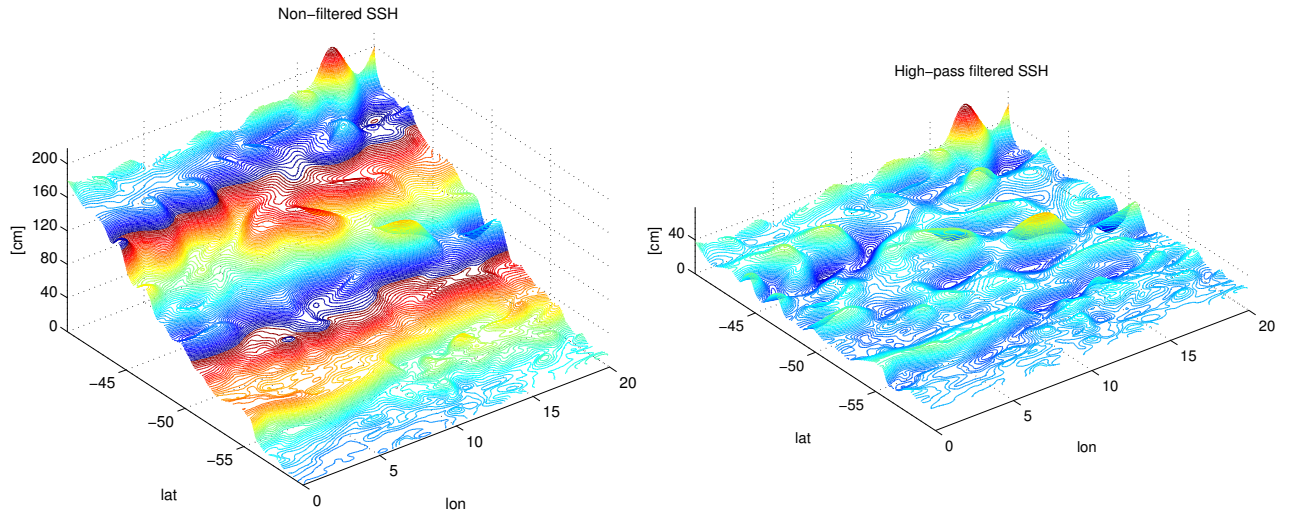


Figure 1.1: SSH with mean over time subtracted.

1.4 Step S03: Find Contours

```
function S03_contours
```

The sole purpose of this step is to apply MATLAB's `contourc.m` function to the SSH data. It simply saves one file per time-step with all contour indices appended into one vector². The contour intervals are determined by the user defined increment and range from the minimum- to the maximum of given SSH data.

The function `initialise.m`, which is called at the very beginning of every step, here has the purpose of rechecking the *cuts* for consistency and correcting the time-steps accordingly (*i.e.* when files are missing). `initialise.m` also distributes the files to the threads *i.e.* parallelization is in time dimension.

² see the MATLAB documentation.

1.5 Step S04: Filter Eddies

```
function S04_filter_eddies
```

Since indices of all possible contour lines at chosen levels are available at this point, it is now time to subject each and every contour to a myriad of tests to decide whether it qualifies as the outline of an eddy as defined by the user input threshold parameters.

1.5.1 Reshape for Filtering and Correct out of Bounds Values

```
function eddies2struct
function CleanEddies
```

In the first step the potential eddies are transformed to a more sensible format, that is, a structure `Eddies(EddyCount)` where `EddyCount` is the number of all contours. The struct has fields for level, number of vertices, exact *i.e.* interpolated coordinates and rounded integer coordinates.

The interpolation of `contourc.m` sometimes creates indices that are either smaller than 0.5 or larger than $N + 0.5$ ³ for contours that lie along a boundary. After rounding, this seldomly leads to indices of either 0 or $N + 1$. These values get set to 1 and N respectively in this step.

³ where N is the domain size

1.5.2 Descent/Ascend Water Column and Apply Checks

```
function walkThroughContsVertically
```

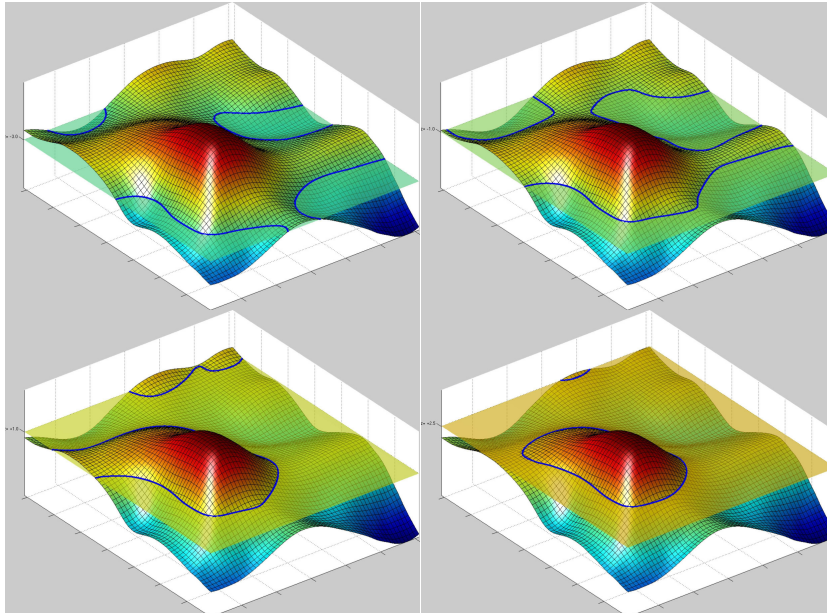


Figure 1.2: TODO:YO!

The concept of this step is a direct adaption of the algorithm described by Chelton *et al.* [2]. It is split into two steps, one for anti-cyclones and one for cyclones. Consider *e.g.* the anti-cyclone

situation. Since all geostrophic anti-cyclones are regions of relative high pressure, all anti-cyclones⁴ effect an elevated SSH *i.e.* a *hill*. The algorithm ascends the full range of SSH levels where contours were found. Consider an approximately Gaussian shaped AC that has a peak SSH of say 5 increments larger than the average surrounding waters. As the algorithm approaches the sea surface from below, it will eventually run into contours that are closed onto themselves and that encompass the AC. At first these contours might be very large and encompass not only one but several ACs and likely also cyclones, but as the algorithm continues upwards found contour will get increasingly circular, describing some outer *edge* of the AC. Once the contour and its interior pass all of the tests the algorithm will decide that an AC was found and write it and all its parameters to disk. The AC's region *i.e.* the interior of the contour will be flagged from here on. Hence any inner contour further up the water column will not pass the tests. Once all AC's are found for a given time-step, the SSH flags get reset and the entire procedure is repeated only this time *descending* the SSH-range to find cyclones. The tests for cyclones and anti-cyclones are identical except for a factor -1 where applicable. In the following the most important steps of the analysis are outlined.

⁴ abbreviated AC henceforth

Contour filter 1 NaN-Check Contour

```
function CR_RimNan
```

The first and most efficient test is to check whether indices of the contour are already flagged. Contours within an already found eddy get thereby rejected immediately.

Contour filter 2 Closed Ring

```
function CR_ClosedRing
```

Contours that do not close onto themselves are obviously not eligible for further testing.

Contour filter 3 Sub-Window

```
function get_window_limits, EddyCut_init
```

For further analysis a sub-domain around the eddy is cut out of the SSH data. These functions determine the indices of that window and subtract the resultant offset for the contour indices.

Contour filter 4 Logical Mask of Eddy Interiour

```
function EddyCut_mask
```

Basically this function creates a **flood-fill** logical mask of the eddy-

interior. This is by far the most calculation intensive part of the whole filtering procedure. A lot more time was wasted on attempting to solve this problem more efficiently than time could have been saved would said attempts have been successful. The current solution is basically just MATLAB's `imfill.m`, which was also used in the very first version of 09/2013. EDIT: `imfill.m` was replaced by using `inpolygon.m` to determine which indices lie within the contour-polygon. This method seems to be more exact at determining whether the inside-part of one grid cell (with respect to the smooth, spline-interpolated contour) is larger than the outside part or not.

Contour filter 5 Sense

```
function CR_sense
```

All of the interior SSH values must lie either above or below current contour level, depending on whether anti-cyclones or cyclones are sought.

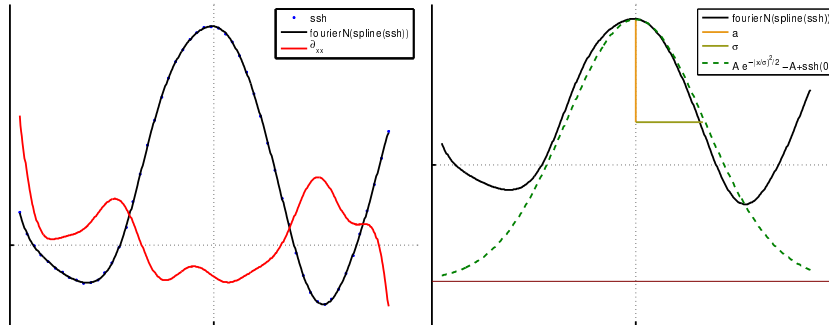


Figure 1.3: Left: Fourier-fit of an eddy from POP-SSH-data and the 2nd differential thereof. Right: Theoretical Gauss-Shape built from the resulting *standard-deviation i.e. σ* and amplitude.

Contour filter 6 Area

```
function getArea
```

The main goal here is to determine the area encompassed by the exact coordinates of the contour. It does so via MATLAB's `polyarea` function. This area is not related to the scale σ that is determined in 12. It is however the relevant scale for the determination of the isoperimetric quotient in 8.

If the respective switch is turned on, this function also checks that the area of found contour does not surpass a given threshold which in turn is a function of L_R . Since L_R gets very small in high latitudes a lower bound on the L_R used here should be set as well. This is especially important for the southern ocean where L_R gets very small

while the strong meso-scale turbulence of the Antarctic circumpolar current results in an abundance of relatively large eddies as far south as 60°S and beyond.

Contour filter 7 Circumference

`function EddyCircumference`

Circumference *e.g.* line-length described by the contour. This is the other parameter needed for 8. This is however neither related to the actual eddy scale determined in 12.

Contour filter 8 Shape

`function CR_Shape`

This is the crucial part of deciding whether the object is *round enough*. A perfect vortex with $\frac{\partial u}{\partial y} = -\frac{\partial v}{\partial x}$ is necessarily a circle. The problem is that eddies get formed, die, merge, run into obstacles, get asymmetrically advected etc. To successfully track them it is therefore necessary to allow less circle-like shapes whilst still avoiding to *e.g.* count 2 semi merged eddies as one. This is achieved by calculating the *isoperimetric quotient*, defined as the ratio of a ring's area to the area of a circle with equal circumference. Chelton *et al.* [2] use a similar method. They require:

*The distance between any pair of points within the connected region must be less than a specified maximum Chelton *et al.* [2].*

While this method clearly avoids overly elongated shapes it allows for stronger deformation within its distance bounds.

Contour filter 9 Amplitude

`function CR_AmpPeak`

This function determines the amplitude *i.e.* the maximum of the absolute difference between SSH and current contour level and the position thereof as well as the amplitude relative to the mean SSH value of the eddy interior as done by Chelton *et al.* [2]. The amplitude is then tested against the user-given threshold. The function also creates a matrix with current contour level shifted to zero and all values outside of the eddy set to zero as well.

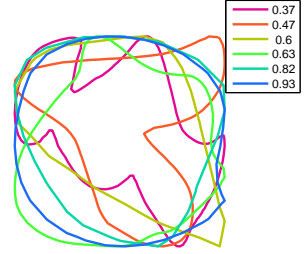


Figure 1.4: Different values of the isoperimetric quotient.

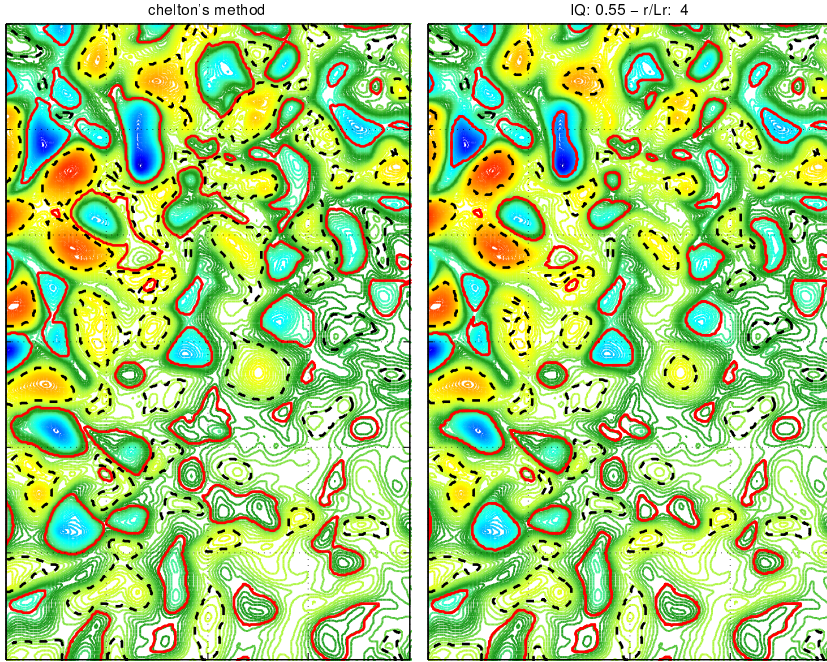


Figure 1.5: Left: The Chelton-method expects to detect eddies at their base and is rather tolerant with respect to the form of found contour. The IQ - method aims more at detecting single round vortices without expecting found contour to be necessarily related to any howsoever-defined outer edge of the eddy.

Contour filter 10 Chelton's Scales

```
function cheltStuff
Chelton et al. [2] introduced 4 different eddy-scales.
```

1. The effective scale L_{eff} as the radius of a circle with its area equal to that enclosed by the contour.
2. The scale L_e as the radius at $z \equiv e^{-1}a$ with a as the amplitude with reference to the original contour and the z -axis zero-shifted to that contour. In other words the effective scale of the contour that is calculated at $1/e$ of the original amplitude.
3. The scale $L = L_e/\sqrt{2}$.
4. The scale L_s which is a direct estimate based on the contour of SSH within the eddy interior around which the average geostrophic speed is maximum [2]. It is hence conceptually the same as σ . This scale was not calculated here, as we could not think of an efficient, simple way to estimate the area bounded by maximum geostrophic speed i.e. the zero-vorticity contour. To understand why this

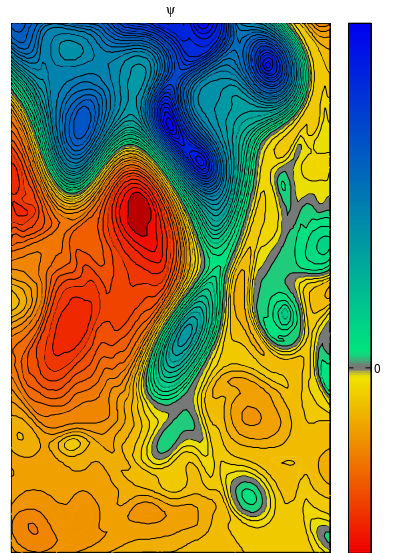


Figure 1.6: Stream function of a meandering jet shedding off a vortex. The line of strongest gradient i.e. fastest geostrophic speed later becomes the zero-vorticity-line at a theoretical distance σ from the center (Offset of Ψ is chosen arbitrarily).

would be difficult to achieve see also sections... **TODO:ref to approp sections eg noise in vort etc.**

Contour filter 11 Profiles

`function EddyProfiles`

This step

- saves the meridional and zonal profiles of SSH, U and V through the eddie's peak and spanning the entire sub-domain as described in 4.
- creates spline functions from the ssh-profiles and uses them to interpolate the profiles onto 100-piece equi-distant coordinate vectors to build smooth interpolated versions of ssh-profiles in both directions.
- in turn uses the splined data to create smooth 4-term Fourier-series functions for the profiles.

Contour filter 12 Dynamic Scale (σ)

`function EddyRadiusFromUV`

The contour line that is being used to detect the eddy is not necessarily a good measure of the eddy's *scale* i.e. it doesn't necessarily represent the eddy's outline very well. This becomes very obvious when the area, as inferred by 6, is plotted over time for an already successfully tracked eddy. The result is not a smooth curve at all. This is so because at different time steps the eddy usually gets detected at different contour levels. Since its surrounding continuously changes and since the eddy complies with the testing-criteria the better the closer the algorithm gets to the eddy's peak value, the determined area of the contour jumps considerably between time steps. This is especially so for large flat eddies with amplitudes on the order of 1cm. If the contour increment is on that scale as well, the difference in contour-area between two time steps easily surpasses 100% and more. Since there is no definition for the *edge* of an eddy, it is defined here as the ellipse resulting from the meridional (zonal) diameters that are the distances between the first local extrema of orbital velocity (one negative, one positive) away from the eddy's peak in y- (x-) directions⁵. In the case of a meandering jet with a maximum flow speed at its center, that is shedding off an eddy, this scale corresponds to half the distance between two opposing center-points of the meander. It is also the distance at which a change in vorticity-polarity

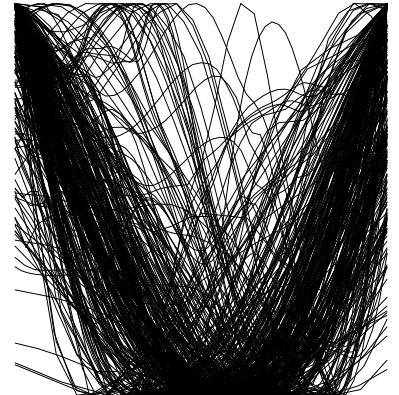


Figure 1.7: Zonal x- and z-normalized cyclone-profiles (early data ~ '13/12).

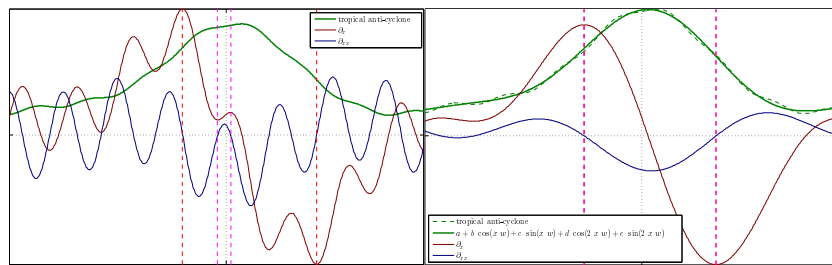
⁵ The velocities are calculated from the gradients of 4th-order Fourier fits to the SSH profile in respective direction (see **TODO:ref**).

occurs and is thus assumed to be the most plausible dividing line between vortices.

Trying to determine the location where this sign change in vorticity occurs in the profiles turns out to be very tricky. What we seek are local extrema of the geostrophic speeds *i.e.* of the ssh-gradients h_x . In a perfect Gaussian-shaped eddy, these would simply correspond to the first local extrema of h_x away from the peak. In *reality* the eddies can be very wobbly with numerous local maxima and minima in the gradients of their flanks. One could argue, that it must be the largest extrema, as it is the highest geostrophic speeds that are sought. In practice⁶ multiple superimposed signals of different scales often create very strong gradients locally. But the main issue here is that one weak eddy adjacent to one strong eddy also has the stronger gradients of the stronger one within its domain so that simply looking for the fastest flow speeds along the profiles is insufficient. It is also not possible to restrict the cut domain to the extent of a single eddy only, because at the point where the domain is selected, we do not know yet whether the detection algorithm *took bait* at the eddy's base or later close to the tip.

The best method thus far seems to be to use the Fourier-series functions from 11 to determine the first extrema away from the eddy's peak. The Fourier order was chosen to be 4 by trial and error. The effect is that small-scale low-amplitude noise is avoided, allowing for more reliable determinations of $\nabla^2 h_{fou} = 0$

Once the zero crossings in all 4 directions are found, their mean is taken as the eddy's scale.



⁶especially for the high-resolution model data.

Figure 1.8: A flat wobbly low-latitude eddy resulting in multiple zero-crossings of its ∇^2 . The problem is addressed by differentiating the profile's Fourier-Series fit instead.

Contour filter 13 Dynamic Amplitude

```
function EddyAmp2Ellipse
```

As mentioned above, the contour that helps to detect the eddy is not representative of its extent. This is also true for the z-direction, for the

same reasons. This function therefor takes an SSH-mean at indices of the ellipse created by the determined zonal and meridional *dynamical* diameters, and uses this as the basal value to determine a *dynamic* amplitude.

Contour filter 14 Center of Volume (CoV)

```
function CenterOfVolume
```

Instead of using the geo-position of the eddy's peak in the tracking procedure, it was decided to instead use the center of the volume created by the basal shifted matrix from 9 *i.e. the center of volume of the dome (resp. valley) created by capping off the eddy at the contour level*. This method was chosen because from looking at animations of the tracking procedure it became apparent that, still using peaks as reference points, the eddy sometimes jumped considerably from one time step to the next if two local maxima existed within the eddy. E.g. in one time-step local maximum A might be just a little bit larger than local maximum B and one time-step later a slight shift of mass pushes local maximum B in pole position, creating a substantial jump in the eddy-identifying geo-position hence complicating the tracking procedure.

Contour filter 15 Geo Projection

```
function ProjectedLocations
```

An optional threshold on the distance an eddy is allowed to travel over one time-step is implemented in the tracking algorithm 1.5. This is a direct adaptation of the ellipse-based constraint described by Chelton *et al.* [2]. The maximum distance in western direction traveled by the eddy within one time-step is limited according to $x_{west} = \alpha c \delta t$ with c as the local long-Rossby-wave phase-speed and

e.g. $\alpha = 1.75$. In eastern direction the maximum is fixed to a value of *e.g.* $x_{east} = 150\text{km}$. This value is also used to put a lower bound on x_{west} and for half the minor axis (y -direction) of the resultant ellipse.

This function builds a mask of eligible geo-coordinates with respect to the next time-step.

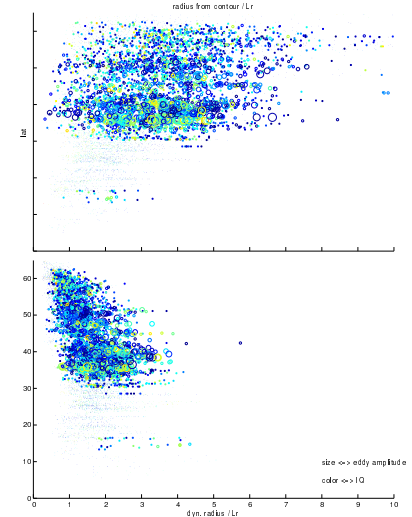


Figure 1.9: Eddies in the North-Atlantic. Y-axis: latitude. X-axis top: ratio of *radius of circle with equal area to that of found contour* to local Rossby-radius. X-axis bottom: ratio of σ to local Rossby-radius. Color-axis: Isoperimetric Quotient. Size: amplitude. The bottom plot suggests that a ratio of say 4 for σ/L_R should be a reasonable threshold. Same graph for the Southern Ocean looks very different though (not shown here), in that said ratio often exceeds ratios as high as 10 and larger in the far south where L_R becomes very small. This problem was addressed by prescribing a minimum value $L_R = 20\text{km}$ for the calculation of the scale-threshold.

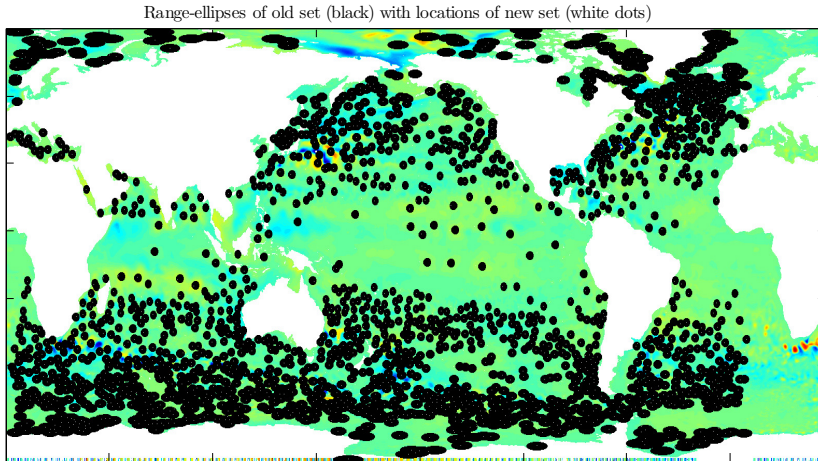


Figure 1.10: Among the saved meta-information for each eddy are also the indices describing the ellipse that defines the eddy's allowed locations with respect to the next time-step.

1.6 Step S05: Track Eddies

S05_track_eddies

1.6.1 Main Tracking Procedure

Due to the relatively fine temporal resolution (daily) of the model data, the tracking procedure for this case turns out to be much simpler than the one described by Chelton *et al.* [1]. There is almost no need to project the new position of an eddy, as it generally does not travel further than its own scale in one day. This means that one eddy can usually⁷ be tracked unambiguously from one time step to the next as long both time-steps agree on which eddy from the other time-step is located the least distance away. The algorithm therefore simply builds an arc-length-distance matrix between all old and all new eddies and then determines the minima of that matrix in both directions *i.e.* one array for the new with respect to the old, and one for the old with respect to the new set. This leads to the following possible situations:

- Old and new agree on a pair. I.e. old eddy O_a has a closest neighbour N_a in the new set and N_a agrees that O_a is the closest eddy from the old set. Hence the eddy is tracked. N_a is O_a at a later time.
- N_a claims O_a to be the closest, but N_b makes the same claim. I.e.

⁷ The only exception being the situation when one eddy fades and another emerges simultaneously and in sufficient proximity.

two eddies from the new set claim one eddy from the old set to be the closest. In this situation the closer one is decided to be the old one at a later time-step and the other one must be a newly formed eddy.

- At this point all new eddies are either allocated to their respective old eddies or assumed to be *newly born*. The only eddies that have not been taken care of are those from the old set, that *lost* ambiguity claims to another old eddy, that was closer to the same claimed new eddy. I.e. there is no respective new eddy available which must mean that the eddy just *died*. In this case the entire track with all the information for each time step is archived as long as the track-length meets the threshold criterium. If it doesn't, the track is abandoned.

1.6.2 Improvements

The former is the core of the tracking algorithm. It is almost sufficient by itself as long as the temporal resolution is fine enough. The larger the time-step, the more ambiguities arise, which are attempted to be mitigated by flagging elements of the distance matrix not meeting certain thresholds:

- `function checkDynamicIdentity`

Consider the ambiguous case when there are two eddies N_a and N_b in sufficient proximity to eddy O_a . Let's assume O_a is a relatively solid eddy of rel. large scale with a steep slope *i.e.* large amplitude and that N_a is merely a subtle blob of an eddy whilst N_b is somewhat similar to O_a but with only half the amplitude. The situation then is clear: N_b is the, apparently slowly dying, O_a at a later time, while N_a could either be a newly formed eddy, an old eddy with its respective representation in the old set something other than O_a , or even just temporary coincidental noise not representative of any significant meso-scale vortex. This interpretation should hold even when O_a sat right between the other two, thereby being much closer to O_a than N_b was.

The purpose of this step is to make such decisions. It does so by comparing the *dynamic* versions of amplitude and scale (*ampToElliipse* and σ) between the time-steps. If either ratio from new to old⁸ surpasses a given threshold the pair is flagged as non-eligible.

It is important to use the *dynamic* parameters rather than those

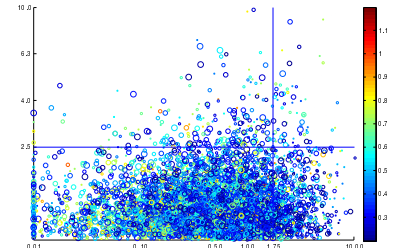


Figure 1.11: Each circle represents one eddy in the new time step. Y-axis: Maximum ratio to closest eddy in old set of either amplitude or σ , where 1 means *identical* and 2 means factor 2 difference. The threshold used for the final runs was 2. X-axis: Ratio of distance to closest eddy from old set divided by δt to local long-Rossby-wave phase-speed. Color-axis: Isoperimetric Quotient. Radius of circles: ratio of σ to local Rossby-radius. All eddies with said ratio larger than 10 are omitted. Note the obvious inverse correlation of scale to IQ, suggesting that all large *eddies* likely represent more than one vortex.

⁸ In order to compare in both directions equally: $\exp(|\log(v_n/v_o)|)$ where v is either amplitude or scale.

stemming from the contour line, because as mentioned in 1.2 the contour line itself and the eddy's geometric *character* are hardly correlated at all. One eddy can get detected at different z-levels from one time-step to the next, resulting in completely different amplitudes, scales and shapes with respect to the contour.

The initial idea was, by assuming Gaussian shapes, to construct a single dimensionless number representing an eddy's geometrical character built upon the contour-related amplitude- and scale values only. Since we have no information about the vertical position of a given contour with respect to assumed Gauss bell, this problem turned out to be intrinsically under-determined and hence useless. The method eventually used, which checks amplitude and scale separately is again very similar to that described by Chelton *et al.* (see Box 1).

- `function nanOutOfBounds`

This is the second half to the prognostic procedure described in 1.6. It simply flags all pairs of the distance matrix for which the index representing the *new* eddy's geographic location is not among the set of indices describing the ellipse⁹ around respective *old* eddy.

⁹ see figure 1.10.

- `function checkAmpAreaBounds`

TODO:relevant only for chelton method!

1.7 Step S06: Cross Reference Old to New Indices

`function S05_init_output_maps`

The output Mercator-maps usually have different geometry from the input maps'. This step allocates all grid nodes of the input data to their respective nodes in the output map. Each output cell will then represent a mean (or median or std) of all input-nodes falling into that *square*.

1.7.1 Running the Code

The separate steps can be run all at once via `Sall.m` or one by one, as long as they are started consecutively in the order indicated by their name (`S00..`, then `S01..` ifnextchar.etcetc.). `S01b` is not necessary though. Each step saves its own files which are then read by the next step. All output data is saved in the user given root-path from ??.

This concept uses quite a lot of disk space and is also quite substantially slowed by all the reading and writing procedures. The benefits, on the other hand, are that debugging becomes much easier. If the code fails at some step, at least all the calculations up to that step are dealt with and do not need to be re-run. The concept also makes it easy to extend the code by further add-ons.

2

Results

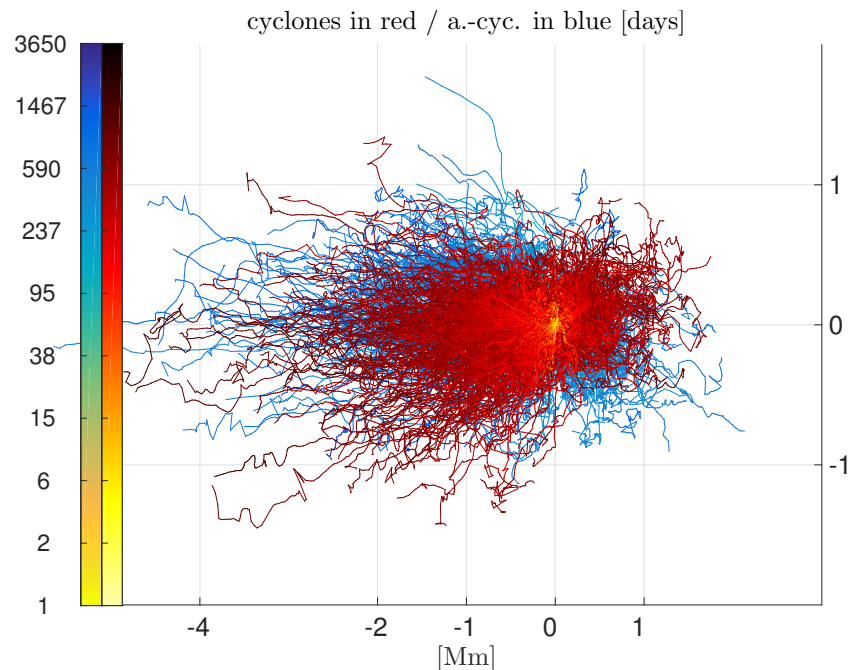


Figure 2.1: aviso-MI: Baseline-shifted
old tracks. Tracks younger than
500 days omitted.

The short time-frame and limited computational resources allowed for only a few complete global runs over the available data. It was therefore critical to carefully choose which method/parameters to use in order to maximize the deducible insight from the results. For best comparability of the results with each other it was decided to agree on one complete set of parameters as a basis, which would then be altered at key parameters. The first run is an attempt to reproduce

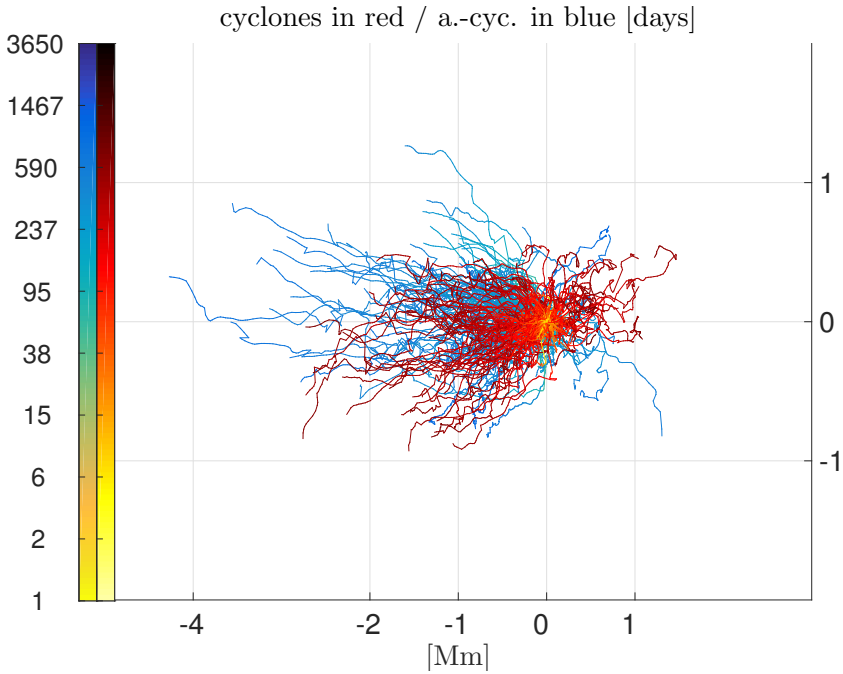


Figure 2.2: aviso-MII: Baseline-shifted old tracks. Tracks younger than 500days omitted.

the results from Chelton *et al.* [2], by setting the algorithm to be the most similar to the algorithm described by ([alias?](#)). The SSH-data for this run is therefor that of the Aviso product. This method will be called **MII**.

The second run is equivalent, except that this time the alternative **IQ**-based shape filtering method from TODO ref and the slightly different tracking-filter as described in TODO ref are used. This setting will be called **MII**. MII is then fed with 7-day time-step POP data as well.

To investigate what role space-resolution plays, the POP data was remapped to that of the Aviso data and fed to the **MII** method. Finally, to investigate the effects of resolution in time, an **MII**/3-day-time-step run over POP data was executed.

Start and end dates were fix for all runs as the intersection of availability of both data sets (see table 2.1 for details).

TODO lookup term used for krummes grid

TODO check tables for completeness

TODO:Cheltons identity check takes Leff?

time frame	1994/01/05 till 2006/12/27
scope	full globe (80S : 80N 180W : 180E)
AVISO geometry	641x1440 true Mercator
POP geometry	2400x3600
contour step	0.01
thresholds	[all SI]
max σ/L_R	4
min L_R TODO	20e3
min IQ	0.55
min data points of an eddy	8
max(abs(rossby phase speed)) TODO	0.2
max amplitude TODO	0.01

Table 2.1: Fix parameters for all runs.

Box 1. Method MI

The concepts used in this method are mostly based on the description of the algorithm described by Chelton *et al.* [2] and all parameters are set accordingly. Basically MI is a modification of MII (which was completed first), with the aim to try to recreate the results from [2]. It differs from MII in the following:

- **detection**

As mentioned in TODO ref, the approach by Chelton *et al.* [2] is to avoid overly elongated objects by demanding:

- **high latitudes**

The maximum distance between any vertices of the contour must not be larger than 400km for $|\phi| > 25^\circ$.

- **low latitudes**

The 400km -threshold increases linearly towards the equator to 1200km .

- **tracking**

The other minor difference to MII is in the way the tracking algorithm flags eddy-pairs between time-steps as sufficiently similar to be considered successful tracking-candidates (see TODO ref). In this method an eddy B from time-step $k+1$ is considered as a potential manifestations of an eddy A from time-step k as long as both - the ratio of amplitudes (with regard to the mean of SSH within the found contour) and the ratio of areas (interpolated versions as discussed in TODO ref) fall within a lower and an upper bound.

Box 2. Method MII

Even though, in its core, directly inspired by Chelton *et al.* [2], this method differs from MII and thus from the description by Chelton *et al.* mainly in the way the shape of a found contour is deemed sufficiently eddy-like.

- **detection**

The IQ -method. See 1.5 and 8.

- **tracking**

Conceptually similar to MI, it is again vertical and horizontal scales that are compared between time-steps. Preferring a single threshold-value over one upper and one lower bound, a parameter ζ was introduced that is the maximum of the two values resulting from the two ratios of amplitudes respective σ , where either ratio is -if larger- its reciprocal in order to equally weight a decrease or an increase in respective parameter. In other words: $\zeta = \max(|\exp|\log R_\alpha|; |\exp|\log R_\sigma||)$, where R are the ratios.

2.1 MI - 7 day time-step - AVISO

THE RESULTS from the MI-method are special in that they feature many long-lived eddies (see Figures 2.1, 2.3 and 2.5), some of which travelled more than 4000 km west. Tracks were recorded throughout the entire world ocean with the only exceptions being an approximately 20° -wide stripe along the equator. The highest count of unique eddies is along the Antarctic Circumpolar Current¹ with

¹ abbreviated ACC from here on.

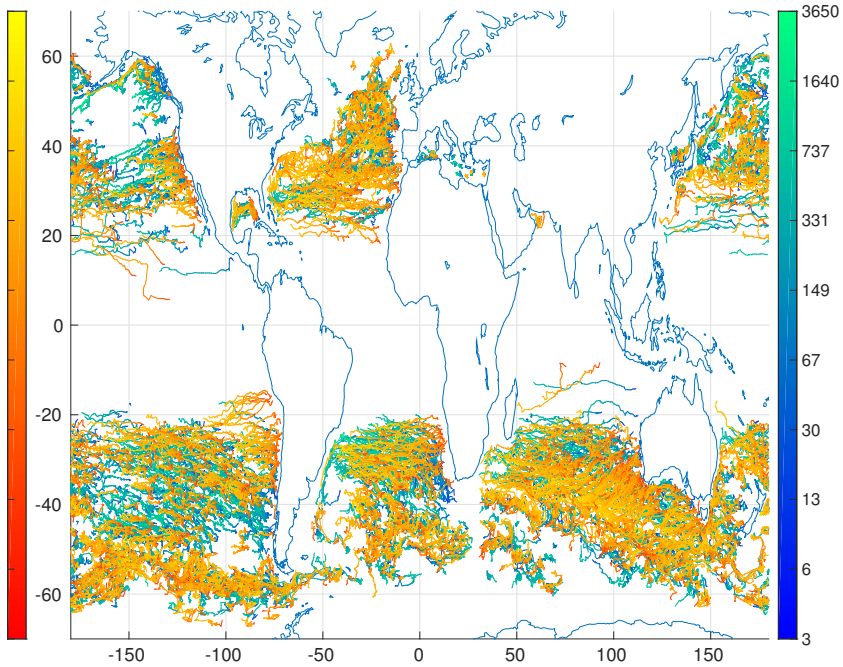


Figure 2.3: MI: anti-cyclones ind red.
Tracks younger than 1a omitted for clarity.

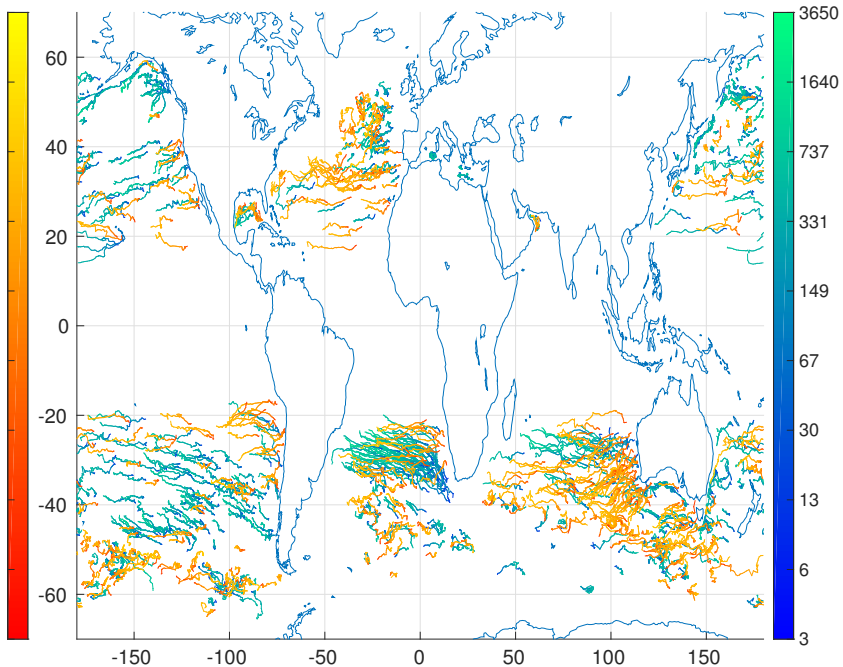


Figure 2.4: MII: anti-cyclones ind red.
Tracks younger than 1a omitted for clarity.

counts of more than 60 individual eddy-visits per $1^\circ \times 1^\circ$ -cell. Further eddy-rich regions are the western North-Atlantic throughout the Gulf-Stream and North-Atlantic Current, *Mozambique eddies* [?] at 20° South along the Mozambique coast, along the Agulhas Current and south of the Cup of Good Hope at $\sim 40^\circ$, along the coasts of Brazil, Chile and all along the Eastern, Southern and Western coasts of Australia (see Figure 2.7).

EDDIES APPEAR AND DISAPPEAR throughout the world ocean. For long-lived solid eddies there is a tendency to emerge along western coasts (see ??).

THE SCALE σ of tracked eddies is similar to that in ?], yet generally smaller in high latitudes and slightly larger in low latitudes (see ??). It is larger than the first-mode baroclinic Rossby Radius by factor of at least 2 and its meridional profile appears to be seperable into two different regimes; one apparently linear profile in low latitudes and a steeper one equatorwards of $\sim |15^\circ|$. Regionall, locations of high meso-scale activity appear to correlate with smaller eddy-scales (see Figure 2.9).

THE EASTWARD ZONAL DRIFT SPEEDS are slightly slower than the first-mode baroclinic Rossby-Wave phase-speed and agree well with the results from ?]. Propagations is generally west-wards except for regions of sufficiently strong eastward advection as in the ACC and North Atlantic Current (see Figure 2.10 and ??).

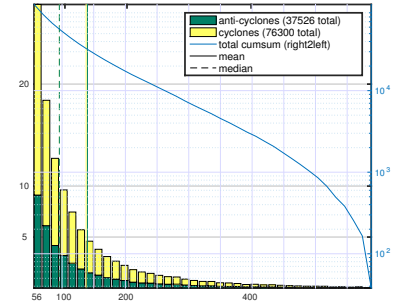


Figure 2.5: [aviso-MI](#) : Final age distribution. x-axis: [days], Left y-axis: [1000]

places of birth and death. size indicates final age.

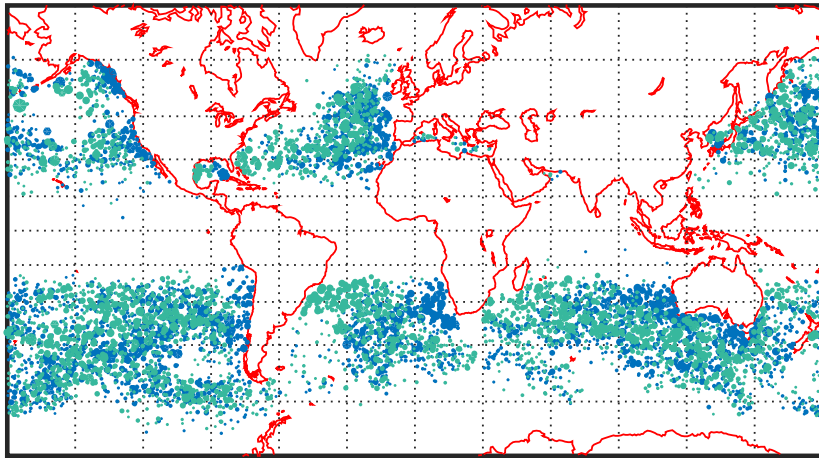


Figure 2.6: **aviso-MI** : Births are in blue and deaths in green. Size of dots scales to age squared. Only showing tracks older than one year.

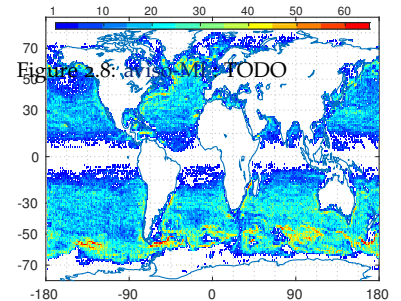
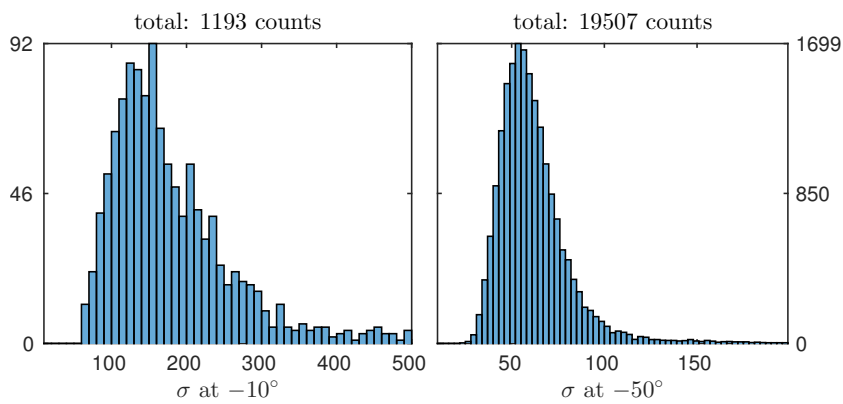


Figure 2.8: **aviso-MI** : Total count of individual eddies per 1 degree square.

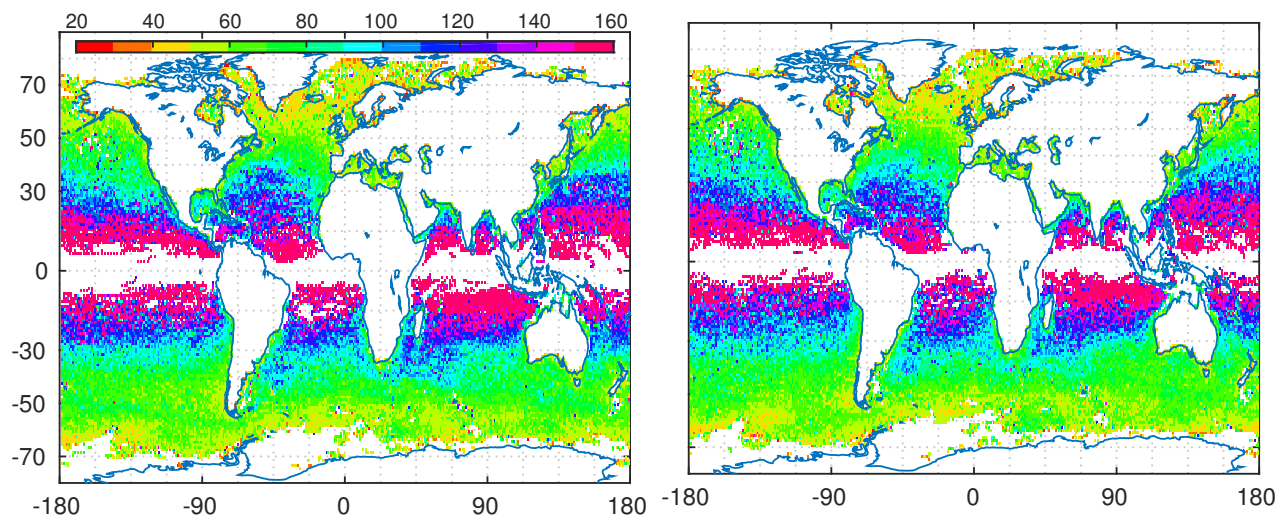


Figure 2.9: aviso-MI : TODO

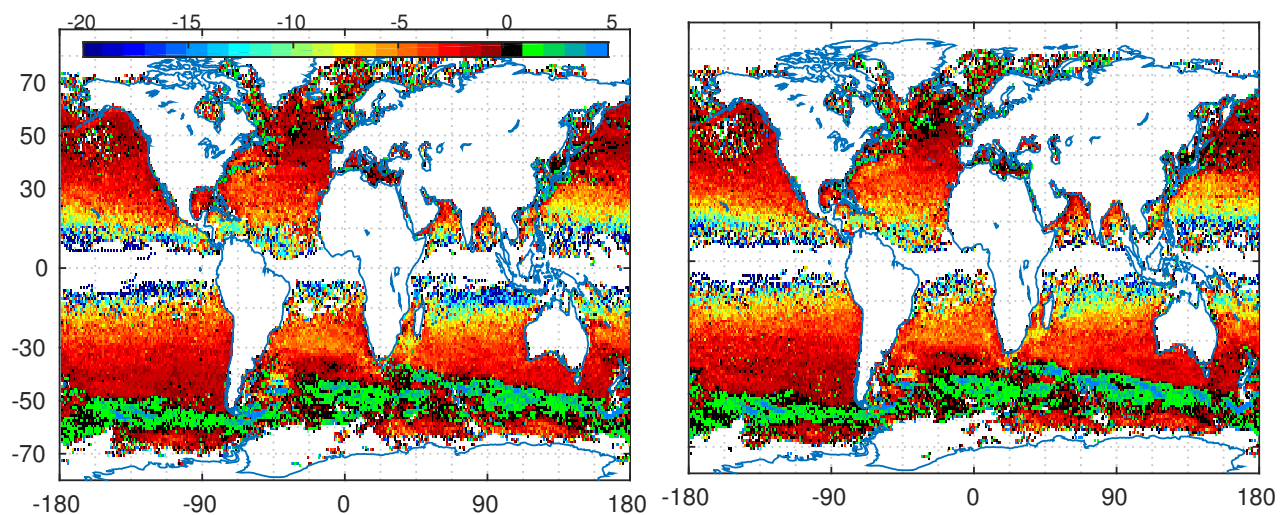


Figure 2.10: aviso-MI : TODO

2.2 MII - 7 day time-step - AVISO

THE IQ -BASED METHOD results in approximately the same total amount of tracks as the MI-method used in section 2.1 (see Figures 2.5 and 2.11). The difference is that tracks here are generally much shorter, meaning that less eddies are detected at any given point in time.

THE SCALE σ is now smaller than that from ?] for all latitudes in zonal- mean as well as median.

WESTWARD DRIFT SPEEDS are almost identical to those in Section 2.1.

places of birth and death. size indicates final age.

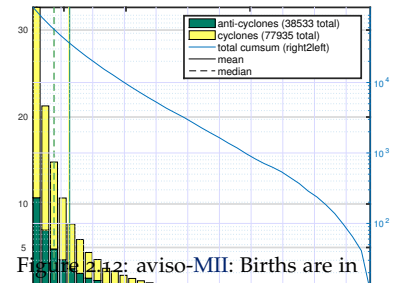
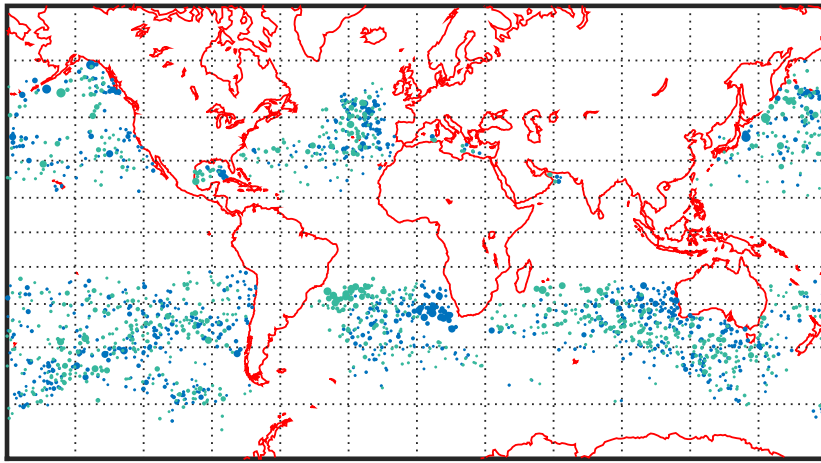


Figure 2.12: aviso-MII: Births are in blue and deaths in green. Size of dots scale to age squared. Only showing tracks older than one year. Left y-axis: [1000]

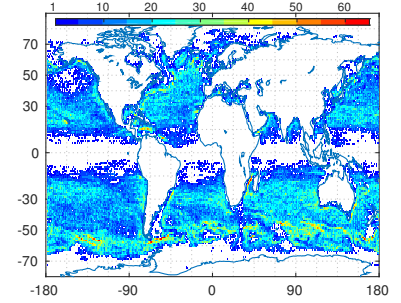


Figure 2.13: aviso-MII: Total count of individual eddies per 1 degree square.

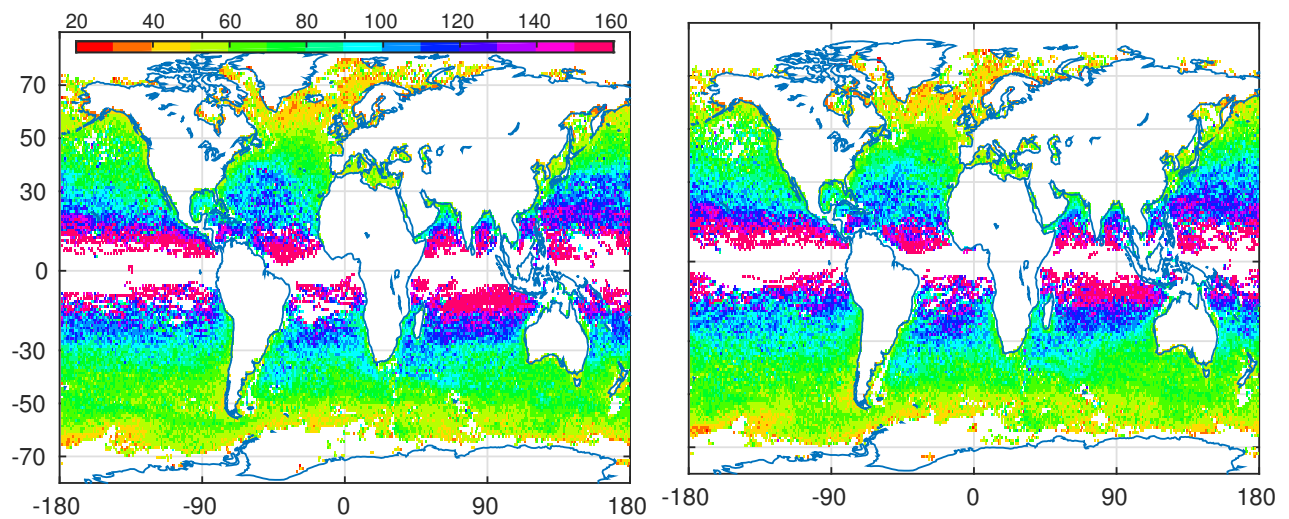


Figure 2.14: aviso-MII: TODO

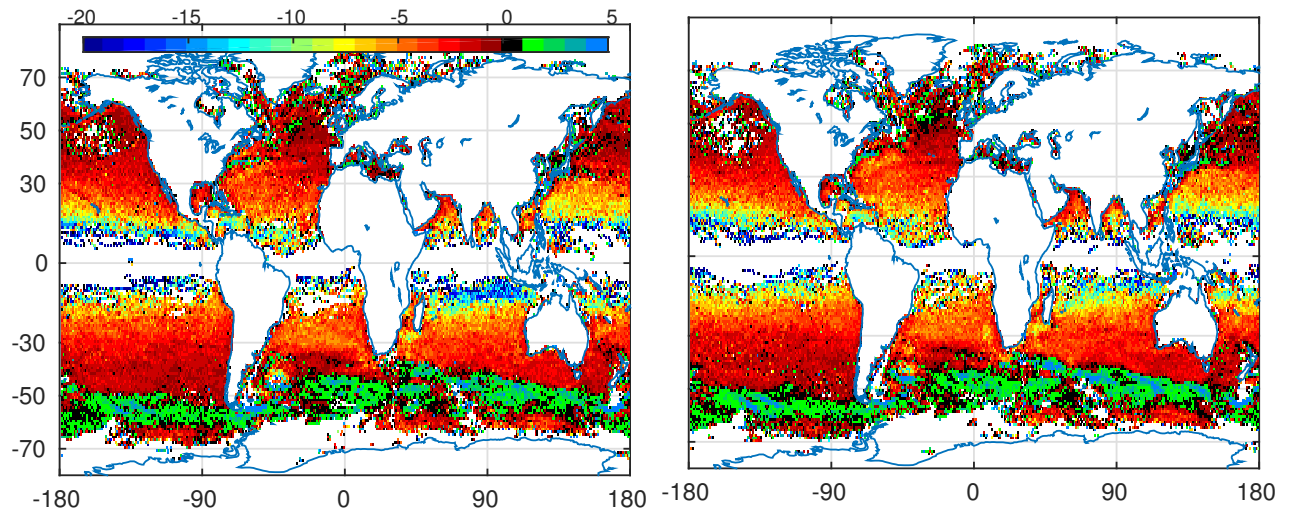


Figure 2.15: aviso-MII: TODO

2.3 MII - 7 day time-step - POP

THE MODEL DATA delivers slightly more total tracks with a similar 2-fold dominance of cyclones over anti-cyclones (compare Figures 2.11 and 2.16). Similar to [aviso-MII](#) very long tracks are fewer than via [aviso-MI](#)². The regional pattern looks somewhat similar to the satellite patterns in terms of which regions feature the strongest eddy activity, with the exception of an unrealistic abundance of eddies right along the Antarctic coast where no eddies were detected for the satellite data likely due to sea ice and/or the inherent lack of polar data due to the satellites' orbit-inclinations. The more important difference between model- and satellite regional distributions is that the model results indicate significantly less eddy activity away from regions of strong SSH gradients, in the open ocean away from coasts and strong currents. The algorithm also detects hardly any eddy tracks in tropical regions (see ??).

² [aviso-MI](#) features 3000 tracks that are older than 400 days, while both [MII](#) methods have only ~ 1000 of such.

THE SCALE σ is generally smaller for the model-data based analysis than for any satellite-based analyses, especially so in high latitudes.

WESTWARD DRIFT SPEEDS look regionally similar to those from satellite data (figs. 2.15 and 2.19). In the zonal mean their magnitude is below those from satellite (see Figure 2.22).

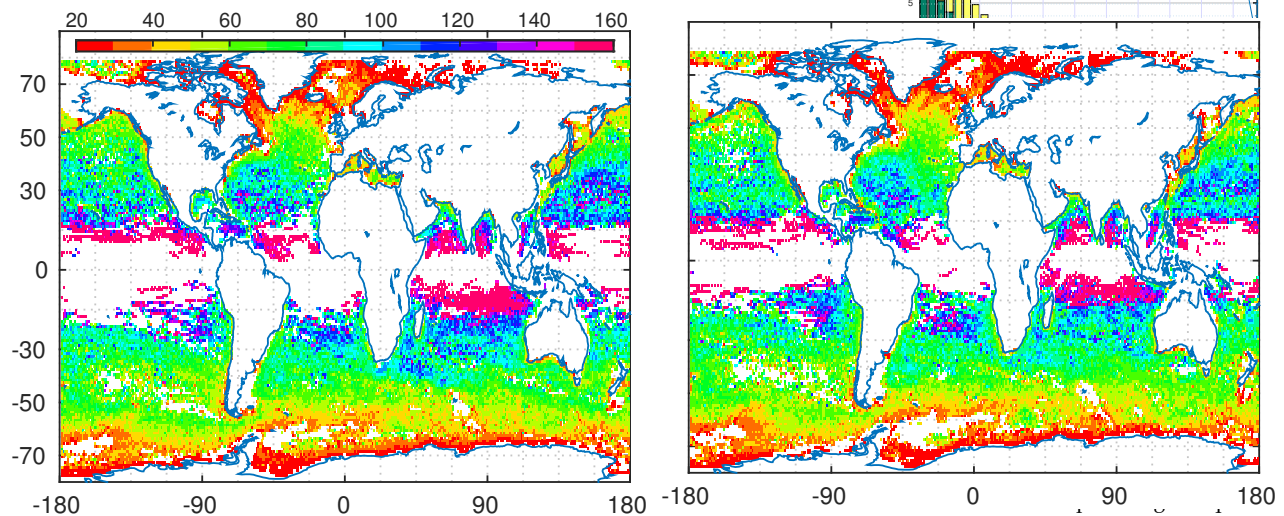


Figure 2.18: pop7-MII: TODO

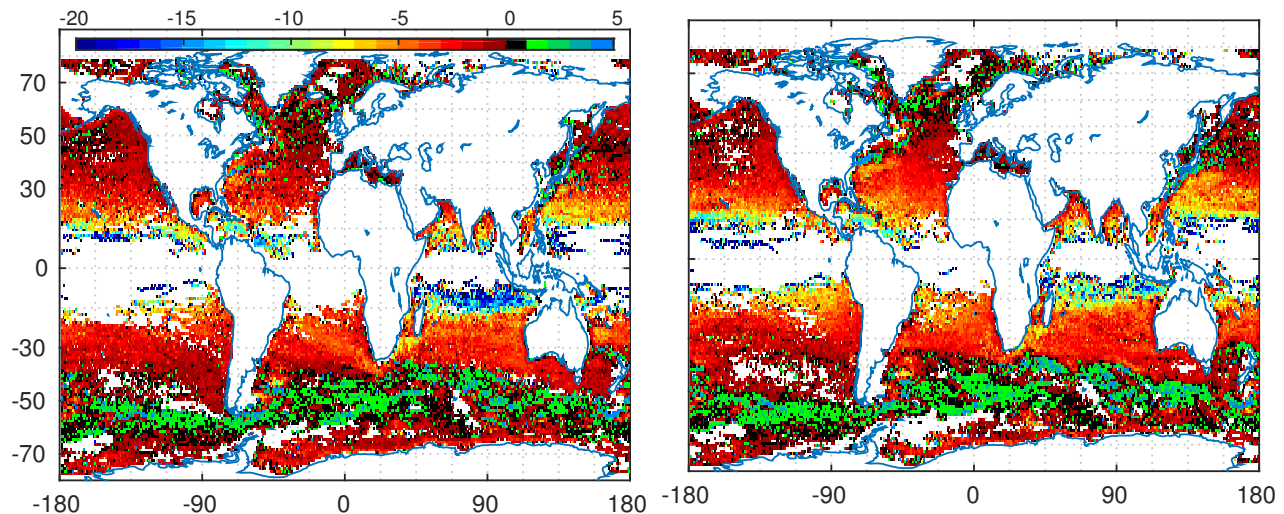


Figure 2.19: pop7-MII: TODO

2.4 MII - 7 day time-step - POP remapped to AVISO geometry

THE MODEL DATA

THE SCALE σ

WESTWARD DRIFT SPEEDS

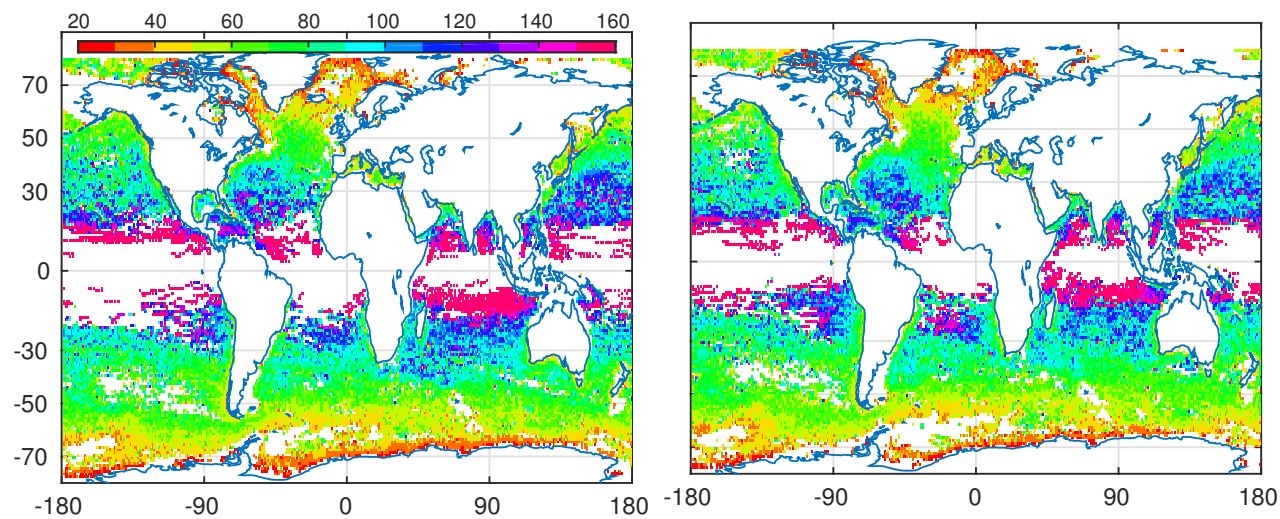


Figure 2.20: pop2aviso-MII: TODO

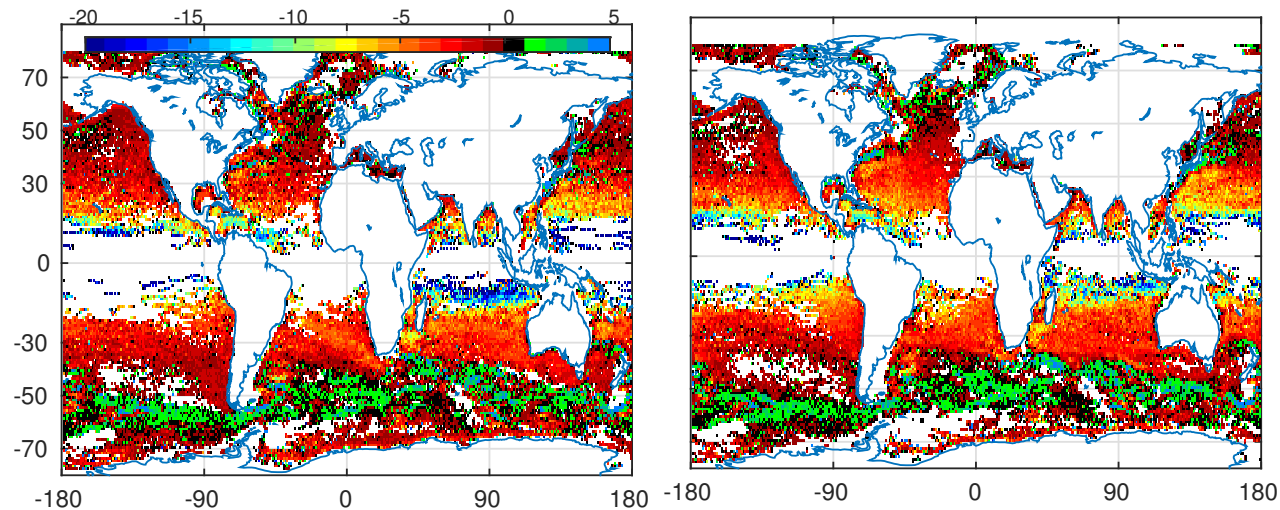


Figure 2.21: pop2aviso-MII: TODO

2.5 MII - 1 day time-step - POP

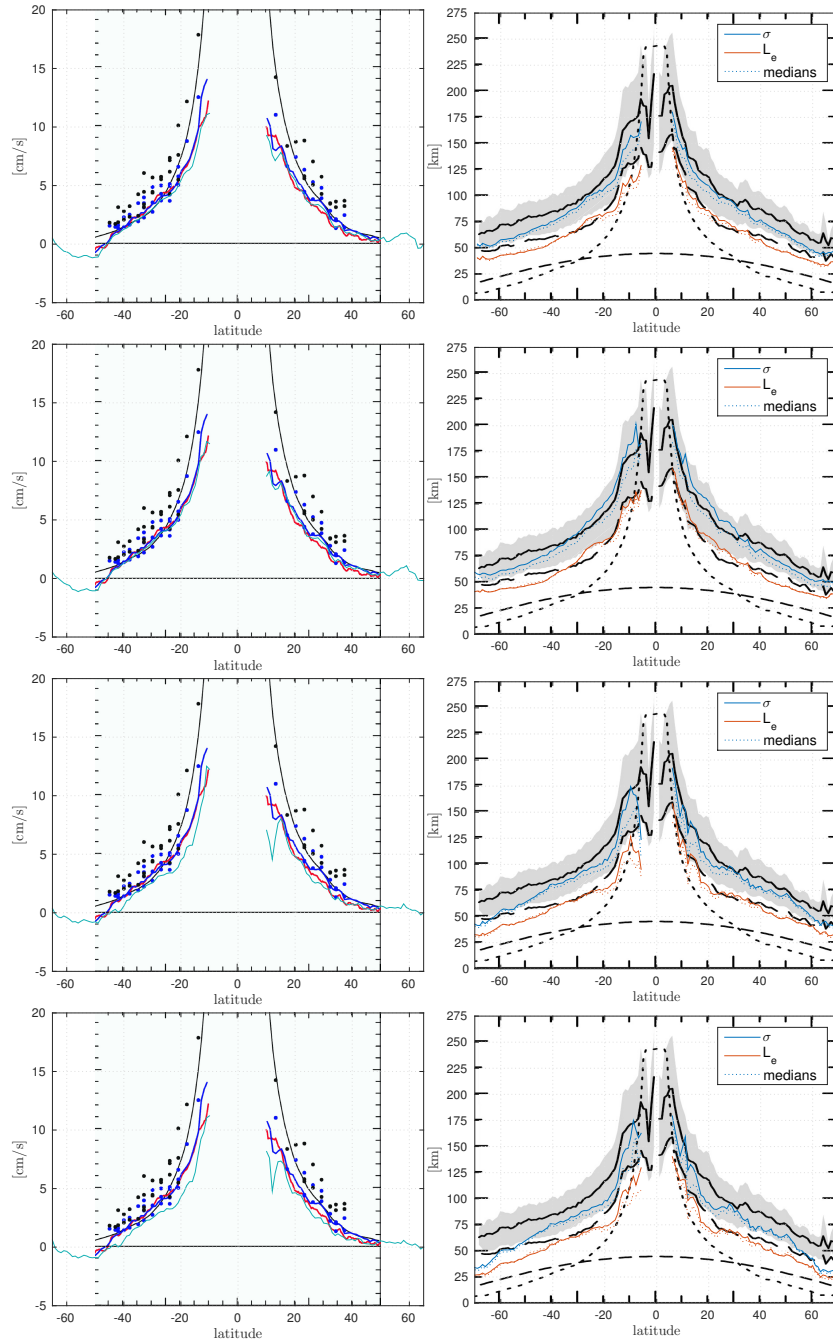


Figure 2.22: Left: Zonal-mean drift speed (cyan) fit to Fig 22 of [2] (Background). Right: σ and L_e fit to Fig. 12 of their paper. Dotted lines are medians instead of means. 1st row: **aviso-MII**, 2nd row: **aviso-MI**, 3rd row: **pop2avi-MII**, 4th row: **POP-7day-MII**. Note that for the very high latitudes ($> |60^\circ|$) the contrast between model and satellite data is further intensified by the lack of satellite data (see figs. 2.14 and 2.18) in those regions (sea-ice / orbit inclinations). For a depiction without this effect see fig. 3.2.

3

Discussion

3.1 Lengths of Tracks

THE MOST APPARENT DIFFERENCE between the [two detection-methods](#) is the abundance of long-lived eddies resulting from the MI-method. The major difference between the two methods is the way in which the *shape* of found contour rings in SSH is decided to be sufficiently *eddy-like* or not (see filter 8).

THE MI-method is the more lenient one, as all it checks for, is whether the contour is of sufficiently compact form. The only shapes that are dismissed are long, thin elongated structures. This means that *e.g.* an eddy-track can more easily ¹ survive situations in which two eddies merge into one or those in which one is split into two or situations in which mean current gradients distort the vortex.

There could also be the situation in which an old, weak eddy fades, yet another one emerges in sufficient proximity. These two events would not even have to coincide at the exact same time, as long as some short-lived coherent structure, of which there is an abundance ² at any given time-step throughout the world ocean, acted as a *bridge* to fill the gap.

THE MII-method is conceptually different in that it is based on the assumption that a distinct coherent vortex need *per definition* to be more or less circular. It will therefore be more likely to regard *e.g.* the situation in which one eddy merges with another one as one of 3 eddies in total; **two** that have just died to create **one** new one. The focus here is more on the propagation of distinct circular

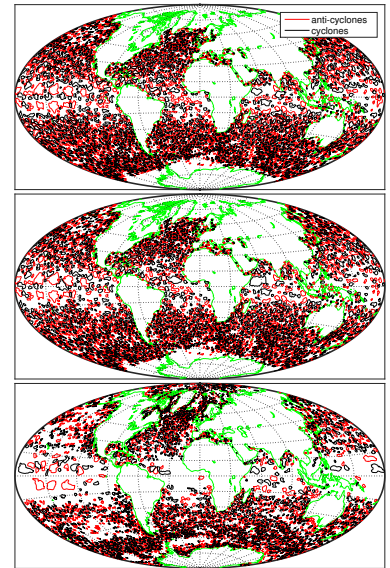


Figure 3.1: All contours that passed the filtering procedure for one exemplary time-step. Top: [aviso-MI](#) . Mid: [aviso-MII](#) . Bottom: [POP-7day-MII](#) .

¹ as long as the similarity-criterion is not violated.

² see ??

geostrophic vortices whereas the focus in the MI-method is more general on coherent local depressions respective elevations in SSH. Unfortunately the time-frame of this work did not allow to test to which degree tracers³ found within tracked eddies remained within the eddy over time. This could further clarify the assumption that the MI-method may be better at tracking water-mass advecting entities, with less jumps between bodies of water within one track.

3.2 Scales

INTERESTINGLY, even in the aviso-MI results, the horizontal eddy scale σ differs from that presented by Chelton *et al.* [2]. For latitudes $\gtrsim |25^\circ|$ the zonal mean here is smaller than theirs while for low latitudes it is higher (see fig. 2.22). The reason for this discrepancy is suspected to stem from the special method by which σ is determined by our **TODO:our? my? this?** algorithm. As outlined in filter 12, here σ is half the mean of zonal and meridional distances between the first two local extrema of the first derivative of interpolated 4th-order fourier fits to the SSH data around the eddy's CoV. The motivation to use fits instead of the SSH directly was on the one hand to avoid noise complicating correct determinations of the 2nd differential zero-crossings and on the other hand to tackle the problem of coarse resolution, especially so for high latitudes where σ seems to become as small as only twice the distance between data points. At this resolution the Gaussian RMS width of an eddy would amount to only 5 data points. Since σ is generally smaller in the higher-resolution POP-data analyses, we hypothesize that the scales by Chelton *et al.* are biased high for high latitudes. Question remains to what degree this bias is inherent to the AVISO product *i.e.* as a smearing effect from the interpolation of multiple coarse satellite data. Or whether it is attributable entirely to the particular method by which the diameter/area of the zero-vorticity contour is estimated.

WITH REGARD to the lower latitudes two important aspects need to be considered:

1. The analyses yield generally low eddy activity in the tropics. Hence the results are less robust in this region *a priori*.
2. The standard deviation in σ is particularly broad in the tropics (see

³ in the model data.

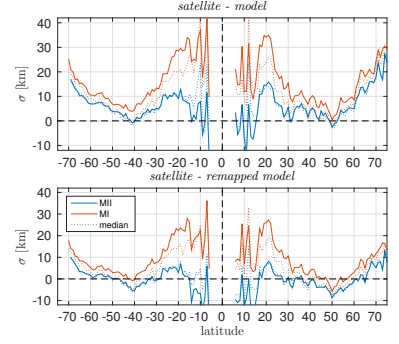


Figure 3.2: Differences in zonal mean σ between AVISO/POP and AVISO-/downsampled POP. Means/Medians are built zonally over only those $1^\circ \times 1^\circ$ -bins that feature data in both sets *i.e.* the intersection of $lat + 1^\circ lon$ of both sets.

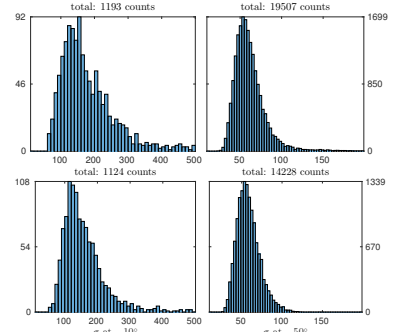


Figure 3.3: Eddy count at one point in time for one fully zonal 1° -bin.
Top: aviso-MI . Bottom: aviso-MII . The tropical spectrum is broad yet with strong positive skewness *i.e.* oriented towards smaller scales. In high latitudes the standard deviation is smaller. The MI method yields more large eddies.

fig. 3.3). As a matter of fact it appears as though there might be two different types of eddies. One type analogous to all high-latitude eddies and a new one of much larger scale. Because these larger eddies have generally low IQ -values they are filtered from the MII analyses, resulting in smaller tropical σ . Their more chaotic shape might, due to the different methods to determine σ , also have to do with why mean tropical σ is larger here than in Chelton *et al.* [2].

THE POP-7day-MII

analysis yields somewhat similar σ for low latitudes⁴, yet significantly smaller values for high latitudes. The question therefore is whether this discrepancy is a re-

sult of the lower resolution of the satellite data *i.e.* that eddies are too small to be resolved by the AVISO product in high latitudes or whether it is attributable to the model data as in a systematic bias due to incomplete/poorly parameterised model physics. This question was the primary motivation for the pop2avi-MII -analysis. The idea here was to down-size the POP data to the geometry of the AVISO grid in order to test whether this would raise σ to that from the satellite results. Figure 3.2 shows that the down-sampling did indeed decrease the discrepancy in σ to respective AVISO analysis, as long as those regions that are unique to either data set are excluded. Between $\pm 25^\circ$ and $\pm 65^\circ$ the difference is no larger than $\pm 5\text{km}$. This came as a surprise because since σ stems from fourier fits of SSH, we expected the original frequencies to be, at least to some extent, conserved in the down-sampled data.

THE MI detection method a priori assumes that an eddy is more or less detected at its asymptotic floor *i.e.* in the case of an anti-cyclone at the *foot of the mountain*. The idea of the IQ -based method on the other hand is to assume that the situation of a single well-defined eddy sitting on an otherwise smooth, flat sea surface, which would be necessary for the contour algorithm to find a closed contour describing the outermost perimeter of said single vortex, is unrealistic. Instead the approach is to look for distinct, sufficiently circular caps

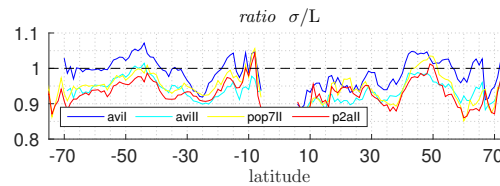


Figure 3.4: Ratios if σ to L (see filter 10)

⁴ Note that due to the lack of tropical eddies the estimates of σ are rather uncertain for the POP analyses.

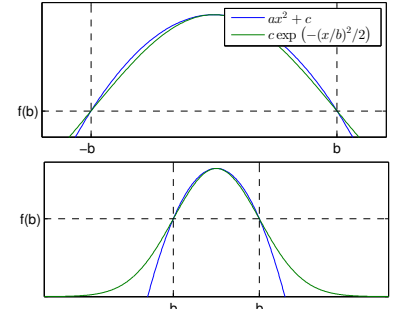


Figure 3.5: The upper part of a Gaussian profile can appear similar to a quadratic one.

of SSH- hills respepective valleys that consistently *wade* through all other weaker geostrophic noise surrounding it. **TODO: why gaussian or quad?**

3.3 Drift Speeds

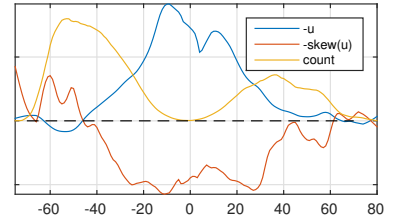


Figure 3.6: TODO

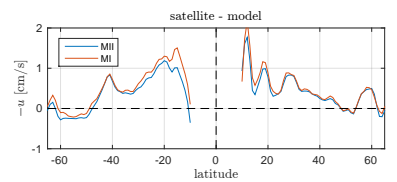


Figure 3.7: TODO:caption

List of Figures

1.1	SSH with mean over time subtracted.	9
1.2	TODO:YO!	10
1.3	Left: Fourier-fit of an eddy from POP-SSH-data and the 2nd differential thereof. Right: Theoretical Gauss-Shape built from the resulting <i>standard-deviation i.e.</i> σ and amplitude.	12
1.4	Different values of the isoperimetric quotient.	13
1.5	Left: The Chelton-method expects to detect eddies at their base and is rather tolerant with respect to the form of found contour. The IQ -method aims more at detecting single round vortices without expecting found contour to be necessarily related to any howsoever-defined outer <i>edge</i> of the eddy.	14
1.6	Stream function of a meandering jet shedding off a vortex. The line of strongest gradient <i>i.e.</i> fastest geostrophic speed later becomes the zero-vorticity-line at a theoretical distance σ from the center (Offset of Ψ is chosen arbitrarily).	14
1.7	Zonal x - and z -normalized cyclone-profiles (early data \sim '13/12).	15
1.8	A flat wobbly low-latitude eddy resulting in multiple zero-crossings of its ∇^2 . The problem is addressed by differentiating the profile's Fourier-Series fit instead.	16

1.9	Eddies in the North-Atlantic. Y-axis: latitude. X-axis top: ratio of <i>radius of circle with equal area to that of found contour</i> to local Rossby-radius. X-axis bottom: ratio of σ to local Rossby- radius. Color-axis: Isoperimetric Quotient. Size: amplitude. The bottom plot suggests that a ratio of say 4 for σ/L_R should be a reasonable threshold. Same graph for the South- ern Ocean looks very different though (not shown here), in that said ratio often exceeds ratios as high as 10 and larger in the far south where L_R becomes very small. This prob- lem was addressed by prescribing a minimum value $L_R =$ 20km for the calculation of the scale-threshold.	17
1.10	Among the saved meta-information for each eddy are also the indices describing the ellipse that defines the eddy's allowed locations with respect to the next time-step.	18
1.11	Each circle represents one eddy in the new time step. Y-axis: Maximum ratio to closest eddy in old set of either ampli- tude or σ , where 1 means <i>identical</i> and 2 means factor 2 dif- ference. The threshold used for the final runs was 2. X-axis: Ratio of distance to closest eddy from old set divided by δt to local long-Rossby-wave phase-speed. Color-axis: Isoperi- metric Quotient. Radius of circles: ratio of σ to local Rossby- radius. All eddies with said ratio larger than 10 are omit- ted. Note the obvious inverse correlation of scale to IQ, sug- gesting that all large <i>eddies</i> likely represent more than one vortex.	19
2.1	aviso-MI: Baseline-shifted <i>old</i> tracks. Tracks younger than 500days omitted.	23
2.2	aviso-MII: Baseline-shifted <i>old</i> tracks. Tracks younger than 500days omitted.	24
2.3	MI: anti-cyclones ind red. Tracks younger than 1a omitted for clarity.	26
2.4	MII: anti-cyclones ind red. Tracks younger than 1a omit- ted for clarity.	26
2.5	bla	27
2.6	aviso-MI : Births are in blue and deaths in green. Size of dots scales to age squared. Only showing tracks older than one year.	28
2.7	aviso-MI : Total count of individual eddies per 1 degree square.	28
2.8	aviso-MI : TODO	28

2.9 aviso-MI : TODO	29
2.10 aviso-MI : TODO	29
2.11 bla	30
2.12 aviso-MII: Births are in blue and deaths in green. Size of dots scales to age squared. Only showing tracks older than one year.	30
2.13 aviso-MII: Total count of individual eddies per 1 degree square.	30
2.14 aviso-MII: TODO	31
2.15 aviso-MII: TODO	31
2.16 bla	32
2.17 pop7-MII: Total count of individual eddies per 1 degree square.	32
2.18 pop7-MII: TODO	32
2.19 pop7-MII: TODO	33
2.20 pop2aviso-MII: TODO	34
2.21 pop2aviso-MII: TODO	34
2.22 Left: Zonal-mean drift speed (cyan) fit to Fig 22 of [2] (Background). Right: σ and L_e fit to Fig. 12 of their paper. Dotted lines are medians instead of means. 1st row: aviso-MII , 2nd row: aviso-MI , 3rd row: pop2avi-MII , 4th row: POP-7day-MII . Note that for the very high latitudes ($> 60^\circ $) the contrast between model and satellite data is further intensified by the lack of satellite data (see figs. 2.14 and 2.18) in those regions (sea-ice / orbit inclinations). For a depiction without this effect see fig. 3.2.	36
3.1 All contours that passed the filtering procedure for one exemplary time-step. Top: aviso-MI . Mid: aviso-MII . Bottom: POP-7day-MII	37
3.2 Differences in zonal mean σ between AVISO/POP and AVISO/downsampled POP. Means/Medians are built zonally over only those $1^\circ \times 1^\circ$ -bins that feature data in both sets <i>i.e.</i> the intersection of $lat + 1i\ lon$ of both sets.	38
3.3 Eddy count at one point in time for one fully zonal 1° -bin. Top: aviso-MI . Bottom: aviso-MII . The tropical spectrum is broad yet with strong positive skewness <i>i.e.</i> oriented towards smaller scales. In high latitudes the standard deviation is smaller. The MI method yields more large eddies.	38
3.4 The upper part of a Gaussian profile can appear similar to a quadratic one.	39
3.5 (see filter 10)	39

3.6	TODO	40
3.7	TODO:caption	40

List of Tables

2.1 Fix parameters for all runs.	24
--	----

4

Bibliography

- [1] Chelton, Dudley B., Schlax, Michael G., Samelson, Roger M., & de Szoeke, Roland a. 2007. Global observations of large oceanic eddies. *Geophys. Res. Lett.*, 34(15), L15606.
- [2] Chelton, Dudley B., Schlax, Michael G., & Samelson, Roger M. 2011. Global observations of nonlinear mesoscale eddies. *Prog. Oceanogr.*, 91(2), 167–216.